Tests and numerical studies on the strain rate effect on compressive strength of recycled aggregate concrete

Jinlong Guo [a, b], Qingjun Chen [b, c *], Wensu Chen [d], Jian Cai [b, c]

[a] *School of Civil Engineering, Fujian Jiangxia University, Fuzhou, 350108, China*

[b] *School of Civil and Transportation Engineering, South China University of Technology, Guangzhou, 510641, China*

[c] *State Key Laboratory of Subtropical Building Science, Guangzhou, 510641, China*

[d] *Centre for Infrastructural Monitoring and Protection, School of Civil and Mechanical Engineering, Curtin University, Kent Street, Bentley, WA 6102, Australia*

Abstract:

The dynamic compressive strength of recycled aggregate concrete (RAC) was studied by conducting quasi-static compression tests and high strain rate tests with split Hopkinson pressure bar (SHPB). The RAC specimens with three recycled coarse aggregate (RCA) replacement percentages of 30%, 70% and 100% and the natural aggregate concrete (NAC) specimen were prepared and tested. The effect of various RCA replacement percentages on the compressive strength under quasi-static and dynamic loads was studied. The failure modes of the specimens after testing were recorded and compared, and the dynamic compressive strength was analyzed. Regression formulae for dynamic increase factor (DIF) on the compressive strength for RAC were proposed. In this study, the DIF of compressive strength ranges from 1 to 3, and increases with the increase of RCA replacement percentage. In addition, the Continuous Surface Cap Model (CSCM) for RAC material is calibrated with the SHPB testing data by numerical simulation. The numerical results show that CSCM with strain rate effect can predict the dynamic compression behavior of RAC with a relatively high precision.

Keywords: Recycled aggregate concrete; Dynamic compressive strength; Strain rate effect; DIF; CSCM

* Corresponding author. E-mail address: qjchen@scut.edu.cn.

1. Introduction

The recycling of waste concrete is beneficial and necessary for the environmental preservation and effective utilization of natural resources, especially considering that the amount of waste concrete has increased enormously in China. The use of recycled coarse aggregate (RCA) obtained from waste concrete in new concrete is a solution to solve the problems of waste concrete and the shortage of raw material. Thus, recycled aggregate concrete (RAC) in which the natural coarse aggregates (NCA) are partially or entirely substituted by the RCA has been gradually studied and used adopted in structure engineering in recent years (Purushothaman et al. 2014; Zhang and Zhao 2014; Li et al. 2015; He et al. 2017; Mwasha and Ramnath 2018). On the other hand, RAC structures may be subjected to impact during their construction stage and service life. Such as, the collapse of building (Gu et al. 2014; Guo et al. 2014), the impact of runaway vehicles on the building caused by accidental collisions (Ferrer et al. 2010), the vertical impact of the helicopter emergency landing on the roof of the building (Mainstone 1966), and the rockfall impact on the protection structures in mountainous areas (Mougin et al. 2005; Delhomme et al. 2005), and et al.

Concrete material exhibits the strain rate effect on compressive strength when it is subjected to impact (Abrams 1917). In other words, the dynamic compressive strength of concrete is different under different strain rates. Split Hopkinson Pressure Bar (SHPB) technique has been widely used in the research on the strain rate effect on the dynamic compressive strength of concrete (Malvern et al. 1985; Ross et al. 1989; Hao et al. 2016). Moreover, Hassan and Wille (2017) conducted the SHPB tests on the ultra-high performance concrete and found that the dynamic compressive strength increased monotonically with the increasing strain rate. Deng et al. (2016) investigated the cellular concrete by using SHPB apparatus. It was found that the dynamic increase effect of the compressive strength of cellular concrete was similar to the ordinary concrete at the strain rate ranging from 70 /s to 140 /s. Chen et al. (2013) reported that the ECC concrete with the strength of 56~73 MPa has less strain rate effect as compared to the ordinary concrete. Liu et al. (2012) tested on the rubber reinforced concrete and Hao et al. (2013) studied the spiral steel fiber reinforced concrete by using the SHPB apparatus. All these studies confirm that concrete is a strain rate sensitive material, but the effect of strain rate on compressive strength varies with each type of concrete. For the RAC material, the compressive strength of RAC is affected by the RCA replacement percentage, *r*, which is defined as the ratio of the RCA mass to the mass of all coarse aggregates. But it should be noted that most of the existing studies focus on the quasi-static compressive behaviors of RAC. Only a limited number of researches studied on its dynamic compressive behaviors and proposed the formulae to describe the dynamic increase effect (Xiao et al. 2015; Lu. et al. 2013). In a word, the dynamic test data is still relatively scarce. Therefore, it is essential to conduct a further research on the dynamic compressive strength of RAC with different RCA replacement percentages under high strain rates, and further to consider the application of RAC material in finite element model.

In this study, quasi-static and dynamic loading tests were carried out for natural aggregate concrete (NAC) and RAC specimens with RCA replacement percentages of 30%, 70% and 100%, respectively. By comparing the quasi-static compressive strength with the dynamic compressive strength, the dynamic increase effects on compressive strength of RAC are analyzed and discussed. Based on the test results, the regression formulae for compressive strength dynamic increase factor (DIF) are given. On this basis, by using the regression formulae, the concrete model CSCM, combined with the strain rate, is verified by finite element code LS-DYNA.

2. Tests on compressive strength of RAC

2.1 Quasi-static compressive strength

2.1.1 Raw materials

The cement used in this study is Ordinary Portland cement of grade 42.5 and the water is portable water. The river sand of Zone 3 (GB/T 14684-2001) with fineness modulus of 2.43 was used as fine aggregate. The local gravel was used as NCA and the selected waste concrete was used as RCA in the concrete mixture. The waste concrete was obtained from a local RCA manufacturing plant in Guangzhou, China with the water absorption of 9.37% and the aggregate size from 5~10mm. The coarse aggregate met the grading requirements (JCJ52-2006). The crush index of the recycled coarse aggregates was 9.4% and the apparent density was 2656 kg/m^3.

2.1.2 Description of the specimens

According to the different replacement percentages of RCA, the RAC specimens can be divided into three types: RAC-30, RAC-70, and RAC-100 which stand for recycled aggregate concrete with RCA replacement percentage of 30%, 70%, and 100%, respectively. Due to the high water absorption of the RCA, some additional water was added to make sure the same effective water-cement ratio (W/C) of 0.40 for the NAC and RAC mixtures. The additional water was calculated for the RAC by the water absorption of RCA under saturated surface dry condition. The related details about the four concrete mixtures are given in Table 1.

Table 1 Ingredients of mixed concrete

Specimen	W/C	Water (kg/m^3)	Cement (kg/m^3)	Sand (kg/m^3)	NCA (kg/m^3)	RCA (kg/m^3)
NAC	0.40	231	578	559	952	0
RAC-30	0.46	263	578	559	667	286
RAC-70	0.53	306	578	560	286	667
RAC-100	0.59	339	578	560	0	953

The quasi-static compressive strength specimens were cast in the cubes with 150×150×150 mm, and the cylinders with 150 mm diameter and 300 mm height, respectively.

2.1.3 Quasi-static testing results

The prepared cube specimens with dimensions 150×150×150 mm were tested under quasi-static compression at a loading rate of 0.5 MPa/s as per the Chinese Standard (GB/T 50081-2002). The quasi-static cubic compressive strength are summarized in Table 2, and normalized with respect to the specimen NAC as below

$$\bar{f} = f_{s} / f_{s0} \tag{1}$$

where f_{s0} is the quasi-static compressive strength of the specimen NAC. The typical failure modes of the cubic specimens under quasi-static test are shown in Fig. 1(a). The vertical crack initiated from the middle of the cubes and extended to the top and bottom sides as the load increases.

Table 2 Quasi-static compressive strength

Specimen		Ultimate load (kN)	Strength, f_s (MPa)	Normalized strength, $\bar{f}$
Cubic	NAC	1325.8	58.9	1.00
	RAC-30	1185.0	52.7	0.89
	RAC-70	974.3	43.3	0.73
	RAC-100	800.2	35.6	0.60
Cylindrical	NAC	765.2	43.3	1.00
	RAC-30	658.8	37.3	0.86
	RAC-70	580.5	32.8	0.76
	RAC-100	470.3	26.6	0.61

The cylindrical specimens with 150 mm diameter and 300 mm height were also tested in compression with the same loading rate as the cubes. The results of the cylinder compression tests are given in Table 2, and the compressive strength is normalized as $\bar{f}$ with respect to the specimen NAC. The typical failure modes of the cylinder specimens under quasi-static test are shown in Fig. 1(b). As the cylindrical specimen has a length-diameter (L/D) ratio of 2.0, the frictional constraint is negligible in the middle part of the specimen. Therefore, the concrete specimen can be considered to be in a state of uniaxial compression. The vertical cracks initiated in the middle of the cylinders with lateral expansion and out-surface shedding. As the load increases, the cracks extended to the top and bottom until the specimens crushed.

As given in Table 2, the compressive strength of RAC is affected by the RCA replacement percentage. The relationship between measured quasi-static compressive strength and RCA replacement percentage, r, is shown in Fig. 2. For the convenience of expression, the value of RCA replacement percentage 0 stands for the NAC. The results show that both the quasi-static cubic and cylindrical compressive strength of RAC decrease with the increase of RCA replacement percentage. Some researches (Otsuki et al. 2003; Nagataki et al. 2004; Liu et al. 2015) have found that the interface transition zone between aggregate and cement mortar determines the mechanical behaviors of

RAC. The compressive strength of RAC is inferior to that of normal concrete due to the reasons including the relatively low strength of interface transition zone, the original defects of voids and cracks in the regeneration process of RCA, and the higher water absorbing ratio of RCA.

Fig. 3 shows the relationship between normalized static compressive strength and RCA replacement percentages. It is found that the normalized quasi-static compressive strength is inversely proportional to the increase of RCA replacement percentages. A regression formula to describe the linear inverse trend is proposed as below

$$\bar{f} = -0.382r + 1 \tag{2}$$

Substituting the Eq. (2) into the Eq. (1), f_s can be expressed as

$$f_s = f_{s0}\left(-0.382r + 1\right) \tag{3}$$

To verify the Eq. (3), a series of RAC cubic specimens with a different water-cement ratio of 0.49 is prepared and tested in quasi-static compression as per Chinese Standard (GB/T 50081-2002). The cubic strengths are given in Table 3 and used to verify the regression formula Eq. (3). As given in Table 3, the maximum error is 5.8% for the RAC-100, which means that Eq. (3) can well predict the quasi-static compressive strength with different RCA replacement percentages.

Table 3 Verification of Eq. (3) for f_s

RCA replacement percentage, r	Test data (MPa)	Predication by Eq. (3) (MPa)	Error (%)
0 (NAC)	30.7	30.7	0
30%	26.5	27.3	3.1
70%	22.3	22.4	0.6
100%	20.2	19.0	-5.8

2.2 Dynamic compressive strength

2.2.1 Description of the SHPB tests

The dynamic compressive tests were conducted using an SHPB apparatus, as shown in Fig. 4(a) and (b). The SHPB test system consists of five parts: a striker bar with 800 mm in length and 37 mm in diameter; a conical variable cross-sectional incident bar with 3200 mm in length (the striking end is 37 mm in diameter and the other end is 74 mm in diameter); a transmitter bar with 1800 mm in length and

74mm in diameter; a cylindrical specimen sandwiched between the incident and the transmitted bars; and a data acquisition system. These bars are made of high-strength alloy steel. The initial impact velocity of the striker bar is recorded by two light transient recorders. The stress waves are measured by the strain gages attached to the surface of the incident and transmitter bars and recorded by the digital oscilloscope at a sampling rate of 500 kHz.

The SHPB testing technique is based on two assumptions as follows. (1) one-dimensional elasticity wave propagates in the incident and transmitter bars; (2) the stress uniformly distributes along the height (Johnson, 1972). In the test, the striker bar impacts against the incident bar. A compressive stress wave is generated by the impact of the striker bar on the incident bar. As shown in Fig. 4 (c), the compressive stress impulse, named as incident wave σ_{I}, propagates through the incident bar and acted on the specimen. Depending on the physical properties of the specimen, the stress impulse is partially reflected into the incident bar in the form of tensile stress impulse, named as reflected wave σ_{R}. The remaining of the stress impulse is transmitted into the transmitter bar, named as transmitted wave σ_{T}. Based on the assumption (1), the stress waves through the top and bottom surfaces of the specimen can be recorded by the strain gages as shown in Fig. 4 (d). The average value of these two stress values is regarded as the representative value according to the assumption (2). The stress, strain and strain rate of the specimen can be derived as below (Johnson, 1972)

$$\begin{cases} \sigma_{\mathrm{s}} = \dfrac{\left(\sigma_1 + \sigma_2\right) A}{2A_{\mathrm{s}}} = \dfrac{\left(\sigma_{\mathrm{I}} - \sigma_{\mathrm{R}} + \sigma_{\mathrm{T}}\right) A}{2A_{\mathrm{s}}} \\ \dot{\varepsilon}_{\mathrm{s}} = \dfrac{v_1 - v_2}{l_{\mathrm{s}}} = \dfrac{v_{\mathrm{I}} + v_{\mathrm{R}} - v_{\mathrm{T}}}{l_{\mathrm{s}}} = \dfrac{C_0}{l_{\mathrm{s}}}\left(\varepsilon_{\mathrm{I}} + \varepsilon_{\mathrm{R}} - \varepsilon_{\mathrm{T}}\right) \\ \varepsilon_{\mathrm{s}} = \int_0^t \dot{\varepsilon}_{\mathrm{s}} \mathrm{d}t = \dfrac{C_0}{l_{\mathrm{s}}} \int_0^t \left(\varepsilon_{\mathrm{I}} + \varepsilon_{\mathrm{R}} - \varepsilon_{\mathrm{T}}\right) \mathrm{d}t \end{cases} \tag{4}$$

where the σ_{s}, ε_{s} and $\dot{\varepsilon}_{\mathrm{s}}$ are the stress, strain and strain rate of the specimen, respectively; l_{s} and A_{s} are the height and cross-section area of the specimen; A and C_0 are the cross-section area and the elastic wave velocity of the bars; v is the nodal velocity; the subscript 1 and 2 denote the top and bottom surface of the specimen, and the subscript I, R and T denote the incident, reflected and transmitted wave, respectively.

Based on the theory of one-dimensional elasticity wave propagation, the stress equilibrium is described as

$$\begin{cases} \sigma_{\mathrm{R}} = \sigma_{\mathrm{I}} - \sigma_{\mathrm{T}} \\ \varepsilon_{\mathrm{R}} = \varepsilon_{\mathrm{I}} - \varepsilon_{\mathrm{T}} \end{cases} \tag{5}$$

Substituting the Eq. (5) into the Eq. (4), the stress state of the specimen can be expressed as

$$\begin{cases} \sigma_{\mathrm{s}} = \dfrac{\sigma_{\mathrm{T}} A}{A_{\mathrm{s}}} = \dfrac{EA}{A_{\mathrm{s}}} \varepsilon_{\mathrm{T}} \\ \dot{\varepsilon}_{\mathrm{s}} = \dfrac{2C_0}{l_{\mathrm{s}}} \left(\varepsilon_{\mathrm{I}} - \varepsilon_{\mathrm{T}} \right) \\ \varepsilon_{\mathrm{s}} = \dfrac{2C_0}{l_{\mathrm{s}}} \displaystyle\int_0^t \left(\varepsilon_{\mathrm{I}} - \varepsilon_{\mathrm{T}} \right) \mathrm{d}t \end{cases} \tag{6}$$

where E is the elastic modulus of the bars.

In this study, a trapezoidal wave with a rising time, t, is chosen as the incident wave. During the rising time, the stress wave travels back and forth for several times named as k within the specimen. As suggested by Yang and Shim (2005), the relative error of the stress (α_{k}), between the top and bottom surfaces can be expressed as below

$$\alpha_k = \frac{2\beta^2 \left[1 - \left(-\dfrac{1-\beta}{1+\beta} \right)^k \right]}{2k\beta - 1 + \left(\dfrac{1-\beta}{1+\beta} \right)^k} \tag{7}$$

with

$$k = \frac{t}{l_{\mathrm{s}} / C_{\mathrm{s}}} \tag{8}$$

and the wave impedance ratio β of specimen and bars can be expressed as below

$$\beta = \frac{\rho_{\mathrm{s}} C_{\mathrm{s}} A_{\mathrm{s}}}{\rho_0 C_0 A_0} \tag{9}$$

where the subscript s and 0 denote the specimen and bars, respectively.

To satisfy the assumption (2) in the SHPB test i.e. the uniformly distributed stress, the relative error of the stress α_k should be low enough. Therefore, the specimen height l_s should be small enough according to the Eqs. (8) and (9). However, to minimize the inertial effect and the effect of end friction at the interface between the specimen and bars, the l_s should not be too low as suggested by the research (Song and Hu, 2005). In this study, the height-diameter ratio of the cylinder specimens was designed as 1 : 2, which has been adopted in the researches conducted by Yan et al. (2002) and Li et al. (2012). As shown in Fig. 5(a), the cylinder with 34 mm in height and 68 mm in diameter, are prepared for SHPB tests. As given in Table 4, the SHPB specimens are named as NAC-*n* for NAC and RAC-*r*-*n* for RAC, where *r* denotes the RCA replacement percentage and *n* stands for different specimens.

Table 4 SHPB testing results

Specimen	Impact velocity, v (m/s)	$\dot{\varepsilon}$ (1/s)	f_d (MPa)	DIF	Specimen	Impact velocity, v (m/s)	$\dot{\varepsilon}$ (1/s)	f_d (MPa)	DIF
NAC-1	5.93	32.0	58.1	1.34	RAC-70-1	4.76	20.6	42.9	1.31
NAC-2	6.76	33.0	64.0	1.48	RAC-70-2	5.42	26.2	49.8	1.51
NAC-3	6.79	34.2	64.7	1.50	RAC-70-3	7.29	28.1	53.1	1.61
NAC-4	8.90	38.8	68.9	1.59	RAC-70-4	8.18	31.3	51.4	1.56
NAC-5	7.49	41.0	69.5	1.60	RAC-70-5	6.68	31.4	55.2	1.68
NAC-6	7.81	41.8	74.1	1.71	RAC-70-6	7.75	38.9	69.8	2.12
NAC-7	7.98	41.9	71.7	1.66	RAC-70-7	9.93	45.0	70.9	2.16
NAC-8	9.07	45.3	79.3	1.83	RAC-70-8	9.60	48.2	85.2	2.59
NAC-9	8.71	48.9	79.6	1.84	RAC-70-9	8.68	51.8	83.5	2.54
NAC-10	8.38	51.3	80.9	1.87	RAC-70-10	9.84	53.6	91.5	2.79
NAC-11	11.31	54.2	83.4	1.93	RAC-100-1	5.53	15.9	33.8	1.27
NAC-12	11.31	57.2	85.2	1.97	RAC-100-2	6.71	16.9	34.0	1.28
NAC-13	11.32	63.4	91.6	2.12	RAC-100-3	6.53	23.7	39.1	1.47
RAC-30-1	5.43	19.1	41.3	1.11	RAC-100-4	6.08	29.1	43.1	1.62
RAC-30-2	5.53	23.5	48.8	1.31	RAC-100-5	8.10	31.4	48.2	1.81
RAC-30-3	8.31	37.0	59.7	1.60	RAC-100-6	7.61	32.1	46.5	1.74
RAC-30-4	7.16	38.9	61.7	1.65	RAC-100-7	6.50	34.4	49.7	1.87
RAC-30-5	8.77	41.5	74.4	2.00	RAC-100-8	8.47	37.5	51.5	1.93
RAC-30-6	10.49	47.7	72.8	1.95	RAC-100-9	7.55	39.9	56.9	2.14
RAC-30-7	8.39	48.9	69.1	1.85	RAC-100-10	6.68	42.6	60.6	2.27
RAC-30-8	9.96	51.6	89.3	2.39	RAC-100-11	7.46	42.7	60.4	2.27
RAC-30-9	10.36	52.3	81.2	2.18	RAC-100-12	7.10	46.6	67.2	2.52
RAC-30-10	9.41	56.9	90.9	2.44	RAC-100-13	9.73	46.8	66.5	2.50
RAC-30-11	9.53	57.0	87.1	2.34	RAC-100-14	8.84	46.9	68.0	2.55
RAC-30-12	11.20	58.2	89.8	2.41	RAC-100-15	10.39	50.2	65.7	2.47
					RAC-100-16	9.85	52.3	73.8	2.77

For the preliminary design, the density and elastic modulus of RAC are given as ρ_s = 2400 kg/m^3 and E_s = 30 GPa, and thus the elastic wave velocity of RAC specimen can be calculated as C_s =

$\sqrt{E_s / \rho_s} = 3536$ (m/s). Similarly, the elastic wave velocity of bars can be calculated as C_0 = $\sqrt{E_0 / \rho_0} = 5139$ (m/s) given the elastic modulus E_0 = 206 GPa and the density ρ_0 = 7800 kg/m^3. The wave impedance ratio β of specimen and bars can be calculated as 0.179 according to the Eq. (9). Ravichandran and Subhash (1994) found that the stress wave reaches uniform distribution when $\alpha_k \leqslant 5\%$. $k \geqslant 6$ can be obtained by substituting β = 0.179 and $\alpha_k \leqslant 5\%$ into the Eq. (7). $t \geqslant 58$ μs can be obtained by substituting $k \geqslant 6$ into the Eq. (8) which means the assumption (2) i.e. uniformly distributed stress can be satisfied if the rising time of the trapezoidal incident wave is longer than 58 μs. In this study, a 1 mm thick copper disk with 14~18 mm diameter is placed at the impact end of the incident bar to reach the desired rising time of trapezoidal incident wave.

2.2.2 Dynamic testing results

In the SHPB test, the impact velocities of the striker bar ranged from 4.76 to 11.32 m/s, corresponding to the strain rate ranging from 15.9 to 63.4 /s. The failure modes of RAC specimens are shown in Fig. 5(b) ~ (d). It can be observed that the specimen fails by the appearance of visible cracks in the middle when the strain rate is relatively low as Fig. 5(b) shown. With the increase of strain rate, the specimen fails by the disintegration of the tested specimens into broken pieces as Fig. 5(c) shown. The specimen is crushed into debris and experienced obviously severe damages at high strain rate as Fig. 5(d) shown. In addition, there are similar in the failure modes between NAC and RAC with different RCA replacement percentages.

The typical incident, reflected and transmitted impulse waves are shown in Fig. 6(a). It can be observed that the rising time of the incident impulse is about 100 μs, which is longer than 58 μs. Based on the Eq. (5), the stress equilibrium is checked and achieved as shown in Fig. 6(b). Based on the Eq. (6), the stress-strain relationship curve of the RAC is established by using the incident wave ε_I and the transmitted wave ε_T. The typical curve is shown in Fig. 7. The peak stress obtained from the curve is defined as dynamic compressive strength f_d. The strain rate $\dot{\varepsilon}$ is taken as the average value of strain rate prior to the peak stress.

The compressive strength increment at high strain rate is defined by dynamic increase factor (DIF) as follows

$$\mathrm{DIF} = f_{\mathrm{d}} / f_{\mathrm{s}} \tag{10}$$

where f_{d} and f_{s} are the concrete uniaxial compressive strength in dynamic and quasi-static loading, respectively. In this study, the cylindrical compressive strength is taken as quasi-static compressive strength f_{s} owing to its uniaxial compression state. The testing data of RAC with the RCA replacement percentages, i.e. the DIF, f_{d}, $\dot{\varepsilon}$ are tabulated in Table 4.

As shown in Fig. 8, the DIFs of the specimens are calculated and plotted against strain rate $\dot{\varepsilon}$. It is found that the RAC is a strain rate sensitive material, which is the same as the NAC. When the strain rate is relatively low, the dynamic compressive strength of the RAC material is slightly higher than the static compressive strength, and the DIF is close to 1.0. With the increase of the strain rate, the dynamic compressive strength of the RAC material increases relative to the static compressive strength, and the DIF is greater than 1. The average values of DIF of NAC and RAC with different RCA replacement percentages are analyzed under different strain rate scopes as shown in Fig. 9. It is obvious that all the DIFs in each strain rate scope show an increasing trend with the increase of RCA replacement percentages in general. Based on Fig. 8 and Table 4, it can be concluded that the DIF of compressive strength ranges from 1 to 3, and increases with the rising RCA replacement percentage by yielding the DIF up to 2.8 when the specimens were tested at strain rate up to 63.4 /s.

3. Model CSCM for RAC

Continuous Surface Cap Model (CSCM) has been intensively used to model the concrete under high strain rate loading in the numerical simulation. The regression formula is implemented to model the increase in compressive strength with the increasing strain rate. In this study, the model CSCM for

RAC is developed by incorporating the regression formula for dynamic compressive strength.

3.1 Existing formulae for DIF

Some existing formulae for predicting the DIF of concrete materials are available in the literature. One of the most commonly used formulae was given by the Comite Euro-International du Beton (CEB-1990) (1993). The DIF, for the two-stage strain rate dependent behavior of concrete, can be given as

$$\mathrm{DIF}=\begin{cases}\left(\dot{\varepsilon}/\dot{\varepsilon}_0\right)^{1.026\alpha_s}, & \dot{\varepsilon}\le 30\mathrm{s}^{-1}\\ \gamma_\mathrm{s}\left(\dot{\varepsilon}/\dot{\varepsilon}_0\right)^{1/3}, & \dot{\varepsilon}> 30\mathrm{s}^{-1}\end{cases}\tag{11}$$

with

$$\alpha_\mathrm{s}=\frac{1}{5+9\left(f_\mathrm{s}/f_\mathrm{s0}\right)}\tag{12}$$

and

$$\lg\gamma_\mathrm{s}=6.156\alpha_\mathrm{s}-2\tag{13}$$

where $\dot{\varepsilon}$ is the strain rate in /s; f_{s0} = 10 MPa; $\dot{\varepsilon}_0$ = -30×10^{-6} /s.

Tedesco and Ross (1998) carried out a series of SHPB tests on different concrete strengths and moistures. A two-stage strain rate dependent behavior was observed. The transition for the two-stage behavior occurs at a strain rate of 63.1 /s, beyond which the DIF increases more significantly with the increase of strain rate. The formulae are given as

$$\mathrm{DIF}=\begin{cases}0.00965\lg\dot{\varepsilon}+1.058\ge 1.0, & \dot{\varepsilon}\le 63.1\mathrm{s}^{-1}\\ 0.758\lg\dot{\varepsilon}-0.289\le 2.5, & \dot{\varepsilon}> 63.1\mathrm{s}^{-1}\end{cases}\tag{14}$$

Based on the results of SHPB tests, Yousef et al. (2015) proposed a simple rational expression, with numerator and denominator being represented by one-degree polynomials as follows

$$\mathrm{DIF}=\left(3.54\dot{\varepsilon}+430.6\right)/\left(\dot{\varepsilon}+447.3\right)\tag{15}$$

Xiao et al. (2015) carried out a series of SHPB tests on RAC specimens with different RCA replacement percentages. A natural logarithm relationship was proposed to describe the relationship of the DIF and the strain rate in the range of 20 /s to 110 /s as follows

$$\mathrm{DIF} = a + b\ln\left(\dot{\varepsilon}\right) \tag{16}$$

where the values of a and b are different for RAC with different RCA replacement percentages.

Another commonly used formula for the DIF that has been implemented into the CSCM (Murray, 2007) for concrete material is given as

$$\mathrm{DIF} = 1 + E\eta_0\dot{\varepsilon}^{(1-n)} / f_\mathrm{s} \tag{17}$$

where E is the elastic modulus; η_0 and n are the strain rate effect parameters.

Based on the literature review, it is indicated that the formulae for the concrete compressive strength DIF have various forms and each one has its own limitation. In addition, the formulae for DIF are various with different mix proportions and grades of the concrete.

3.2 CSCM

The CSCM has been widely used in the numerical simulation of impact response on concrete (Murray et al. 2007; Remennikov and Kong 2012; Guo et al. 2017). To consider the strain rate effect, the DIF incorporated in CSCM is described in the Eq. (17), where the concrete elastic modulus E can be given as below:

$$E = 4700\sqrt{f_s} \tag{18}$$

Based on the Eq. (17), regression formulae for each RCA replacement percentage, r, are derived to describe the relationship between the DIF and the strain rate $\dot{\varepsilon}$ as given in the Eqs. (19) ~ (22) with different parameters η_0 and n.

$$r = 0, \qquad \mathrm{DIF} = 1 + \frac{9.309\times10^{-7}E}{f_\mathrm{s}}\dot{\varepsilon}^{(1+0.817)} \tag{19}$$

$$r = 30\%, \qquad \mathrm{DIF} = 1 + \frac{1.338\times10^{-6}E}{f_\mathrm{s}}\dot{\varepsilon}^{(1+0.763)} \tag{20}$$

$$r = 70\%, \qquad \mathrm{DIF} = 1 + \frac{1.920\times10^{-6}E}{f_\mathrm{s}}\dot{\varepsilon}^{(1+0.710)} \tag{21}$$

$$r = 100\%, \qquad \mathrm{DIF} = 1 + \frac{2.618 \times 10^{-6} E}{f_{\mathrm{s}}} \dot{\varepsilon}^{(1+0.667)} \tag{22}$$

As shown in Fig. 10, the curve from Eq. (19) for the NAC is compared with other curves of the ordinary concrete from the regression formulae by other researches (CEB-1990 1993; Tedesco and Ross 1998; Yousef et al. 2015). It can be seen that the curve from Eq. (19) is close to the regression curves by Tedesco et al. (1998) and Yousef et al. (2015) when the strain rate is lower than 10 /s and close to the curve by CEB-1990 (1993) and Xiao et al. (2015) when the strain rate is higher than 30 /s. The testing data of ordinary concrete in literatures (Abrams 1917; Malvern et al. 1985; Hughes and Watson 1978; Evans 1942; Sparks and Menzies 1973) are scattered and also compared in Fig. 10. The curve from Eq. (19) is in good agreement with the testing data provided by Abrams (1917), Evans (1942) and Sparks and Menzies (1973) when the strain rate is lower than 10 /s, and the ones provided by Malvern et al. (1985) and Hughes and Watson (1978) when the strain rate is higher than 10 /s. Therefore, the Eq. (19) can describe the DIF of ordinary concrete with good accuracy.

The Eqs. (19) ~ (22) can have unified formulation as below

$$\mathrm{DIF} = 1 + \frac{9.309 \times 10^{-7} \bar{\eta}_0 E}{f_{\mathrm{s}}} \dot{\varepsilon}^{(1+0.817\bar{n})} \tag{23}$$

where $\bar{\eta}_0$ and $\bar{n}$ are the normalized strain rate parameters with respect to η_0 and n of the specimen NAC, as tabulated in Table 5. The compressive strength of RAC is affected by the RCA replacement percentage. The regression formulae for $\bar{\eta}_0$ and $\bar{n}$ can be expressed with respect to the RCA replacement percentage r as below

$$\bar{\eta}_0 = 0.730 r^2 + 1.012 r + 1 \tag{24}$$

$$\bar{n} = -0.181 r + 1 \tag{25}$$

The regression curves for $\bar{\eta}_0$ and $\bar{n}$ are plotted in Fig. 11 and they show high correlation.

Table 5 Normalized parameters $\overline{\eta}_0$ and $\overline{n}$

r	η_0	$\overline{\eta}_0$	n	$\overline{n}$
0 (NAC)	9.309×10^{-7}	1.00	-0.817	1.00
30%	1.338×10^{-6}	1.44	-0.763	0.93
70%	1.920×10^{-6}	2.06	-0.710	0.87
100%	2.618×10^{-6}	2.81	-0.667	0.82

Substituting the Eq. (23) into the Eq. (10), f_d can be expressed as

$$f_{\mathrm{d}} = f_{\mathrm{s}} + 9.309\times10^{-7}\,\overline{\eta}_0 E\dot{\varepsilon}^{(1+0.817\overline{n})} \tag{26}$$

where f_s, E, $\overline{\eta}_0$ and $\overline{n}$ can be obtained by the Eqs. (3), (18), (24) and (25), respectively

By using the Eq. (26), the dynamic compressive strength, f_d, of the RAC with the RCA replacement percentages r is plotted against strain rate $\dot{\varepsilon}$ as shown in Fig. 12(a). It is indicated that the dynamic compressive strength of RAC decreases with the increasing RCA replacement percentage when the strain rate is less than 60 /s. As shown in Fig. 12(a), the values of f_d with the different r trend to be closed with the increasing strain rate $\dot{\varepsilon}$, which may be caused by the increasing dynamic increase effect. In addition, the DIF of the RAC with the RCA replacement percentages r is plotted against strain rate $\dot{\varepsilon}$ by using Eq. (23) as shown in Fig. 12(b). It is indicated that the higher RCA replacement percentage leads to higher DIF value, which is consistent with the test result illustrated in Fig. 9. That is the reason for the closed dynamic compressive strength of the RAC with different RCA replacement percentages under high strain rate. Ross et al. (1995) reported that the strain rate sensitivity of concrete may be attributed to the presence of water in the concrete. The compression of the internal pore of concrete is restrained as the water is not able to discharge timely from the internal pore under high strain rate loading, which results in the increasing dynamic compressive strength under high strain rate. In addition, the water content of RCA is higher than that of NCA with no RCA replacement. Therefore, the dynamic increase effect of RAC enhances with the increasing RCA replacement percentage.

3.3 Verification of CSCM for RAC

To verify the CSCM for the RAC, the SHPB test conducted in this study are simulated by using finite element code LS-DYNA. A 3D finite model of the SHPB test is developed as shown in Fig. 13. The RAC specimen and alloy steel bars are modeled as eight-node solid element with one-point Gauss integration. The specimen is divided into 18 equal segments in axial and radial directions, and the bars are divided into 8 equal segments in the radial direction and 25 mm equal segments in the axial direction. The automatic surface to surface contact algorithm is adopted to simulate the contact between bars and specimen. The specimen is very close to the incident and transmitter bars and 2 mm space is kept between the striker bar and the incident bar. The strike bar is applied with an initial impact velocity. An axis-symmetrical numerical model is adopted to save the computational cost. The alloy steel bar is modeled by the elastic model with the elastic modulus of 210 GPa, the Poisson ratio of 0.3 and the density of 7800 kg/m^3. The CSCM is employed to model the RAC with the Poisson ratio of 0.2 and the density of 2400 kg/m^3, and other parameters of the compressive strength are tabulated in Table 6.

Table 6 Parameters of CSCM model

r	f_s (MPa)	E (MPa)	η_0	n
0 (NAC)	43.3	30927	9.309×10^{-7}	-0.817
30%	37.3	28705	1.338×10^{-6}	-0.763
70%	32.8	26918	1.920×10^{-6}	-0.710
100%	26.6	24240	2.618×10^{-6}	-0.667

Two models i.e. the CSCM incorporated with strain rate effect and the CSCM without are used in the numerical simulation. The comparison of the results between the test and numerical results is shown in Fig. 14. It is shown in the figure that except for some individual data, the CSCM incorporated with strain rate effect can give an accurate simulation of the dynamic compressive strength of RAC, especially in the high strain rate region. For the CSCM without strain rate effect considering, it has a certain accuracy in the relatively low strain rate region. But with the strain rate increases, the strength increase is limited, thus the result is lower than the experimental value. Even some numerical value is only about half of the test one. On the whole, the CSCM incorporated with the strain rate effect can provide a more accurate prediction of the dynamic compressive strength of RAC.

4. Conclusions

This paper presents the dynamic compressive properties of recycled aggregate concrete (RAC) by conducting quasi-static and SHPB tests. The dynamic increase effect of RAC is analyzed with the testing results of RAC with the RCA replacement percentages. The RCA replacement percentage has a significant effect on the static and dynamic compressive strength of RAC. With the RCA replacement percentage increasing, both static and dynamic compressive strength of RAC decreases. It is also found that RAC is strain rate dependent. The dynamic increase factor (DIF) ranges from 1 to 3 within the scope of strain rate less than 60 /s, and increases with the RCA replacement percentage. The CSCM model for RAC is developed by incorporating the strain rate effect and the CSCM is verified with the testing data of the SHPB test by using finite element code LS-DYNA. It is proved that the CSCM incorporated with the strain rate effect can provide a more accurate prediction of the dynamic compressive strength of RAC.

Acknowledgments

The authors would like to acknowledge National Natural Science Foundation of China (51578246), Guangdong Province Natural Sciences (2017A030313263) and Australian Research Council (LP150100259) for financial support to carry out this study.

References

Abrams, D. A. (1917). "Effect of rate of application of load on the compressive strength of concrete." *In Proceeding of ASTM*, 17, 364-377.

CEB-1990 (1993). FIP Model Code 1990: Design Code. London, United Kingdom: Thomas Telford.

Chen, Z. T., Yang, Y. Z., and Yao, Y. (2013). Quasi-static and dynamic compressive mechanical properties of engineered cementitious composite incorporating ground granulated blast furnace slag. *Materials and Design*, 44, 500-508.

Delhomme, F., Mommessin, M., Mougin, J.P., and Perrotin, P. (2005). Behavior of a structurally dissipating rock-shed: experimental analysis and study of punching effects. *International Journal of Solids and Structures*, 42(14), 4204-4219.

Deng, Z. P., Cheng, H., Wang, Z. G., Zhu, G., and Zhong, H. (2016). Compressive behavior of the cellular concrete utilizing millimeter-size spherical saturated SAP under high strain-rate loading. *Construction and Building Materials*, 119, 96-106.

Evans, R. H. (1942). Effect of rate of loading on the mechanical properties of some materials. *Journal of the ICE*, 18(7), 296-306.

Ferrer, B., Ivorra, S., Segovia, E., and Irles, R. (2010). Tridimensional modelization of the impact of a vehicle against a metallic parking column at a low speed. *Engineering Structures*, 32(8), 1986-1992.

Gu, X. L., Wang, X. L., Yin, X. J., Lin, F., and Hou, J. (2014). Collapse simulation of reinforced concrete moment frames considering impact actions among blocks. *Engineering Structures*, 65: 30-41.

Guo, J. L., Cai, J., and Chen, W. S. (2017). Inertial effect on RC beam subjected to impact loads. *International Journal of Structural Stability and Dynamics*, 17(4), 1750053.

Guo, J. L., Cai, J., and Chen, Q. J. (2016). Simulation analysis on pancake collapse response of a steel frame under seismic action. *Engineering Mechanics*, 33(06), 171-179.

Hao, H., Hao, Y. F., Li, J., and Chen, W. S. (2016). Review of the current practices in blast-resistant analysis and design of concrete structures. *Advances in Structural Engineering*, 19(8), 1193-1223.

Hao, Y. F., and Hao, H. (2013). Dynamic compressive behaviour of spiral steel fibre reinforced concrete in split Hopkinson pressure bar tests. *Construction and Building Materials*, 48, 521-532.

Hassan, M., and Wille, K. (2017). Experimental impact analysis on ultra-high performance concrete

(UHPC) for achieving stress equilibrium (SE) and constant strain rate (CSR) in Split Hopkinson pressure bar (SHPB) using pulse shaping technique. *Construction and Building Materials*, 144, 747-757.

He, A., Cai, J., Chen, Q. J., Liu, X. P., Huang, P. Z., and Tang, X. L. (2018). Seismic behaviour of steel-jacket retrofitted reinforced concrete columns with recycled aggregate concrete. *Construction and Building Materials*, 158, 624-639.

Hughes, B. P., and Watson, A. J. (1978). Compressive strength and ultimate strain of concrete under impact loading. *Magazine of Concrete Research*, 30(105), 189-199.

Johnson, W. (1972). Impact strength of materials. London, United Kingdom, Edward Arnold.

Li, S., and Hu, S. S. (2005). Stress uniformity and constant strain rate in SHPB test. *Explosion and Shock Waves*, 25(3), 207-216.

Li, W. G., Xiao, J. Z., Shi, C. J., and Poon, C. S. (2015). Structural Behaviour of Composite Members with Recycled Aggregate Concrete - An Overview. *Advances in structural engineering*, 18(6), 919-938.

Li, Z. W., Xu, J. Y., Bai, E. L., and Gao, Z. G. (2012). SHPB test for post-high-temperature concrete. *Journal of Vibration and Shock*, 31(8), 143-147.

Liu, F., Chen, G. X., Li, L. J., and Guo, Y. C. (2012). Study of impact performance of rubber reinforced concrete. *Construction and Building Materials*, 36, 604-616.

Liu, Z., Peng, H., and Cai, C. S. (2015). Mesoscale analysis of stress distribution along itzs in recycled concrete with variously shaped aggregates under uniaxial compression. *Journal of Materials in Civil Engineering*, 27(11), 04015024.

Lu, Y. B., Chen, X., Teng, X., and Zhang, S. (2013). Impact behavior of recycled aggregate concrete based on split Hopkinson pressure bar tests. *Advances in Materials Science and Engineering*, 2013(1), 131-141.

Mainstone, R. J. (1966). Structural tests on an experimental helicopter platform. *Proceedings of the*

Institution of Civil Engineers, 33(1), 65-91.

Malvern, L. E., Jenkins, D. A., Tang, T., and Ross, C. A. (1985). Dynamic compressive testing of concrete. In 2nd Symposium on The Interaction of Non-Nuclear Munitions with Structures, Engineering and Services Laboratory-Tyndall AFB, Panama City Beach, FL, 194-199.

Mougin, J. P., Perrotin, P., Mommessin, M., Tonnelo, J., and Agbossou, A. (2005). Rock fall impact on reinforced concrete slab: an experimental approach. *International journal of impact engineering*, 31(2), 169-183.

Murray, Y. D. (2007). Users manual for LS-DYNA concrete material model 159. Computer Program Documentation.

Murray, Y. D., Abuodeh, A. Y., and Bligh, R. P. (2007). Evaluation of LS-DYNA concrete material model 159. Computer Program Documentation.

Mwasha, A., and Ramnath, R. (2018). Manufacturing concrete with high compressive strength using recycled aggregates. *Journal of Materials in Civil Engineering*, 30(8).

Nagataki, S., Gokce, A., Saeki, T., and Hisada, M. (2004). Assessment of recycling process induced damage sensitivity of recycled concrete aggregates. *Cement and Concrete Research*, 34(6), 965-971.

Otsuki, N., Miyazato, S., and Yodsudjai, W. "Influence of recycled aggregate on interfacial transition zone, strength, chloride penetration and carbonation of concrete." *Journal of materials in civil engineering*, 15.5 (2003), 443-451.

Purushothaman, R., Amirthavalli, R. R., and Karan, L. (2014). Influence of treatment methods on the strength and performance characteristics of recycled aggregate concrete. *Journal of Materials in Civil Engineering*, 27(5), 04014168.

Ravichandran, G., and Subhash, G. (1994). Critical appraisal of limiting strain rates for compression testing of ceramics in a split hopkinson pressure bar. *Journal of the American Ceramic Society*, 77(1), 263-267.

Remennikov, A. M., and Kong, S. Y. (2012). Numerical simulation and validation of impact response of axially-restrained steel–concrete–steel sandwich panels. *Composite Structures*, 94(12), 3546-3555.

Ross, C. A., and Tedesco, J. W. (1989). Split-Hopkinson pressure-bar tests on concrete and mortar in tension and compression. *ACI Materials Journal*, 86(5), 475-481.

Ross, C. A. (1995). Effects of strain rate on concrete strength. *ACI Material Journal*, 92(1), 37-47.

Sparks, P. R., and Menzies, J. B. (1973). The effect of rate of loading upon the static and fatigue strengths of plain concrete in compression. *Magazine of Concrete Research*, 25(83), 73-80.

Tedesco, J. W., and Ross, C. A. (1998). Strain-rate-dependent constitutive equations for concrete. *Journal of Pressure Vessel Technology*, 120(4), 398-405.

Xiao, J. Z., Li, L., Shen, L. M., and Poon, C. S. (2015). Compressive behaviour of recycled aggregate concrete under impact loading. *Cement and Concrete Research*, 71, 46-55.

Yan, S. H., Li, Z. C., Wang, M. Y., and Yin, F. L. (2002). Dynamic compressive behaviour of high-strength steel fiber reinforced concrete. *Explosion and Shock Waves*, 22(3), 237-241.

Yang, L. M., and Shim, V. P. W. (2005). An analysis of stress uniformity in split hopkinson bar test specimens. *International Journal of Impact Engineering*, 31(2), 129-150.

Yousef, A. S., Almusallam, T., Ibrahim, S. M., Abbas, H., and Alsayed, S. (2015). Rate dependent behavior and modeling of concrete based on shpb experiments. *Cement and Concrete Composites*, 55, 34-44.

Zhang, H. R., and Zhao, Y. X. (2014). Performance of recycled aggregate concrete in a real project. *Advances in Structural Engineering*, 17(6), 895-906.

(a) Cubic

(b) Cylindrical

Fig. 1 Failure modes of specimens under quasi-static test

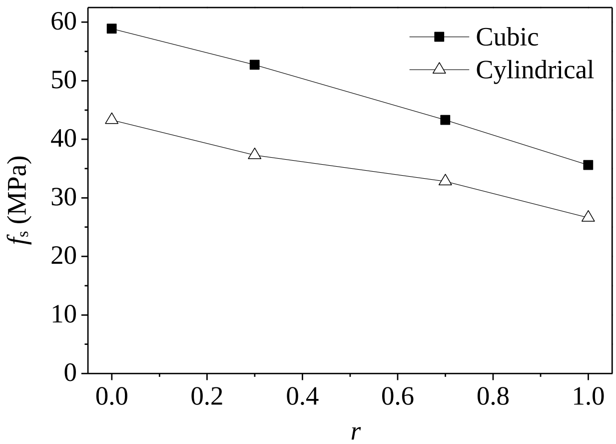

Fig. 2 Quasi-static compressive strength with various RCA replacement percentages

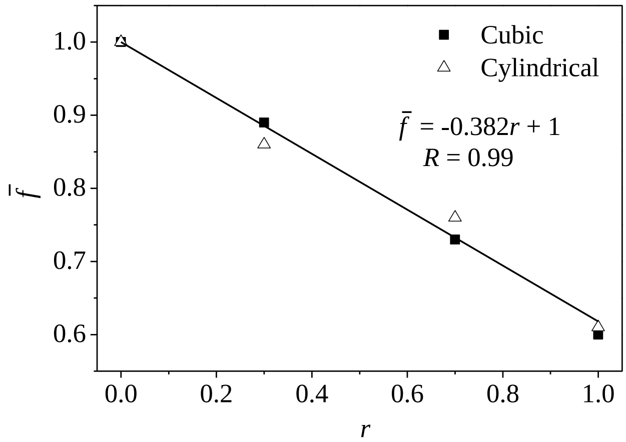

Fig. 3 Normalized quasi-static compressive strength with various RCA replacement percentages

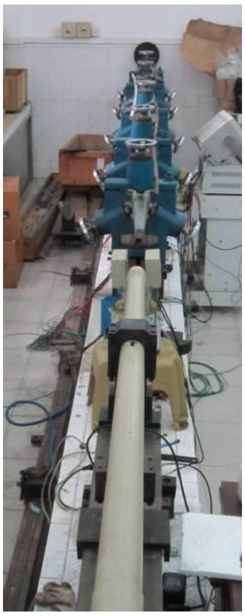

(a) Photograph of SHPB

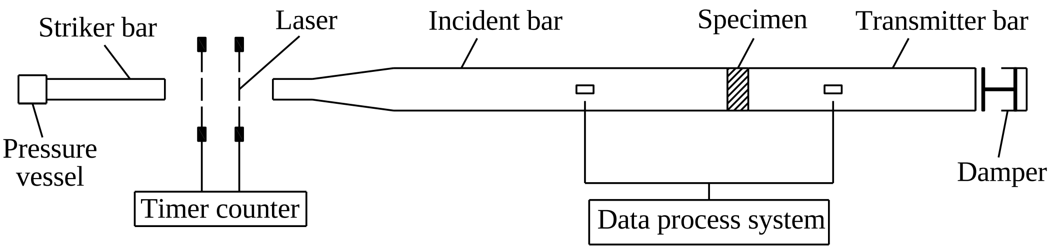

(b) Schematic diagram of SHPB

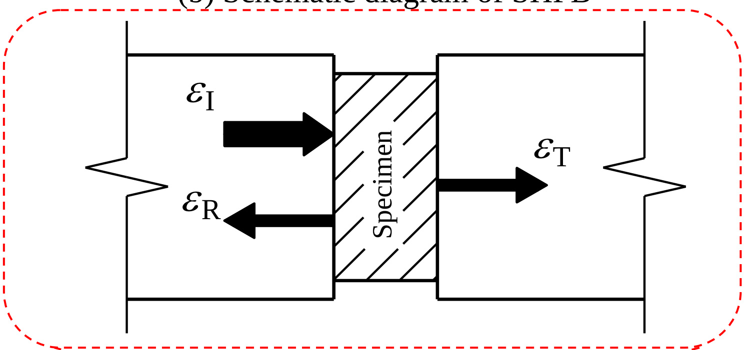

(c) Wave propagation

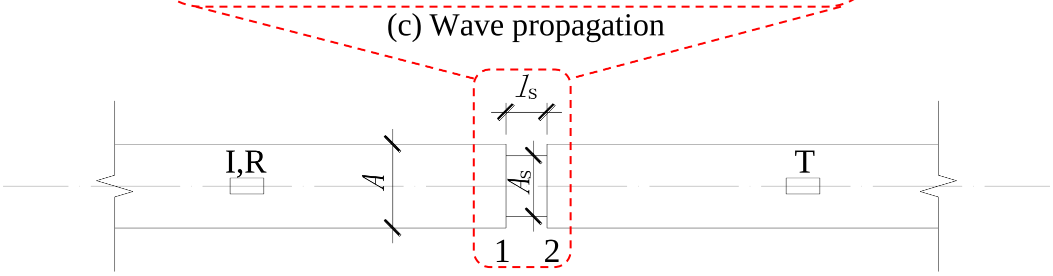

(d) Placement of strain gages

Fig. 4 SHPB testing setup

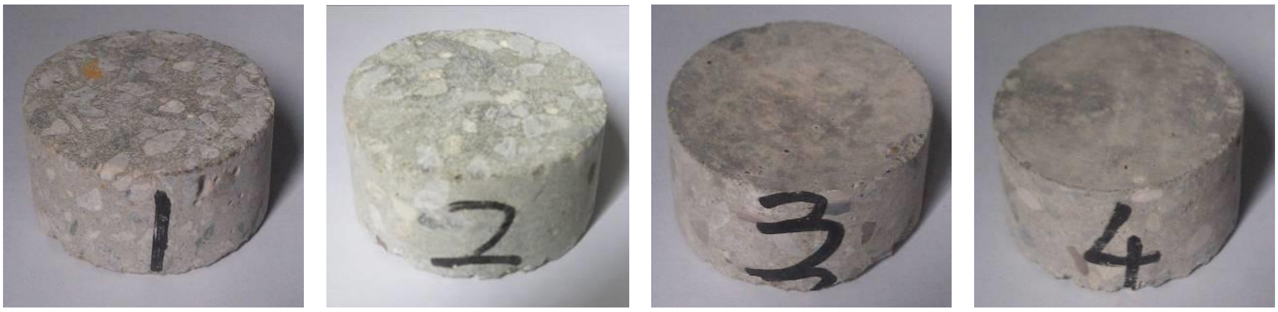

NAC RAC-30 RAC-70 RAC-100

(a)

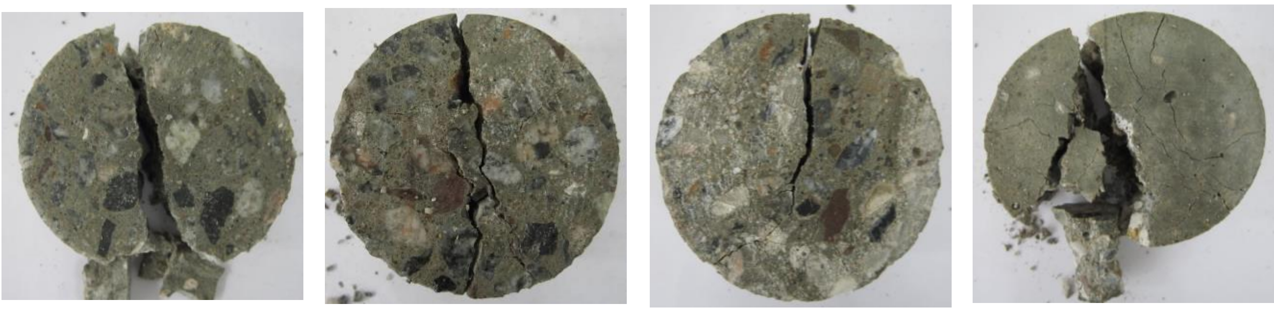

NAC RAC-30 RAC-70 RAC-100

(b)

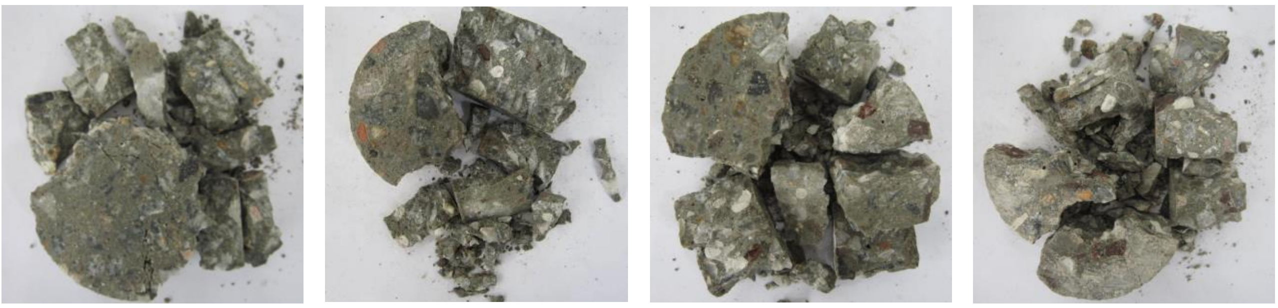

NAC RAC-30 RAC-70 RAC-100

(c)

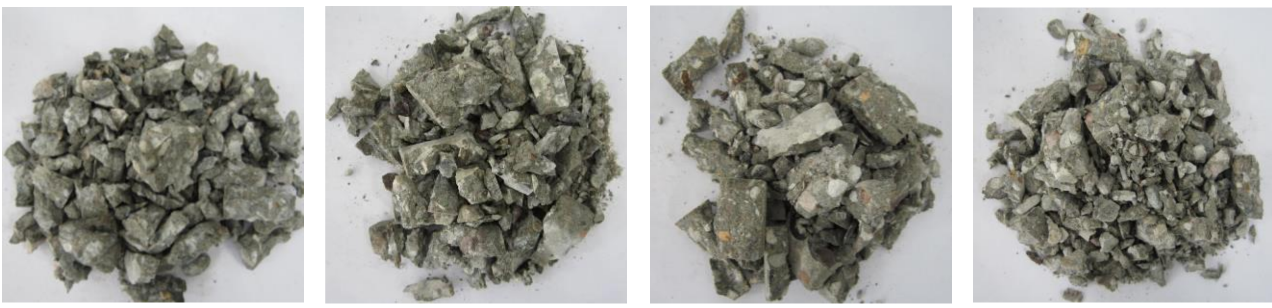

NAC RAC-30 RAC-70 RAC-100

(d)

Fig. 5 SHPB specimens and failure mode

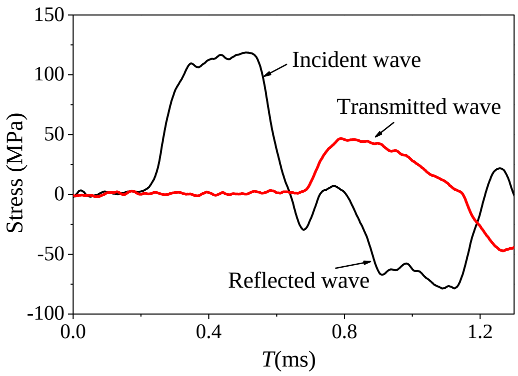

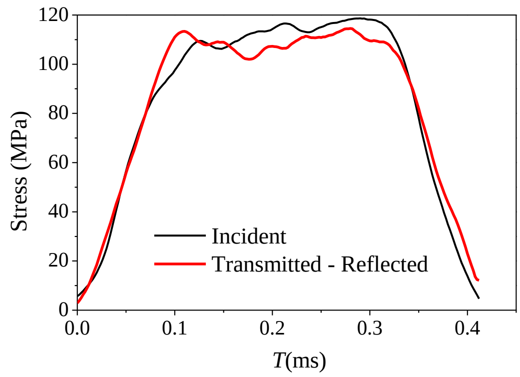

(a) (b)

Fig. 6 Typical impulse waves of SHPB test

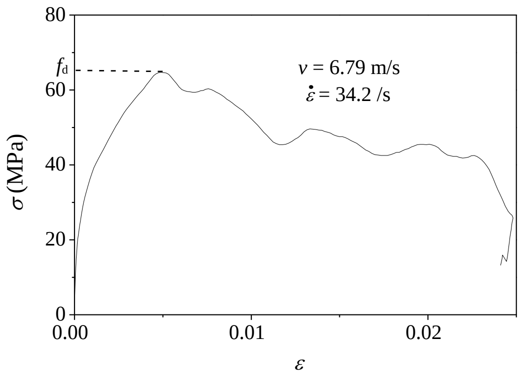

Fig. 7 Typical dynamic stress - strain curve of SHPB specimen

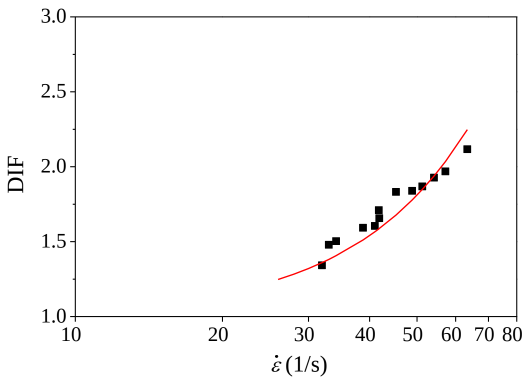

(a) NAC

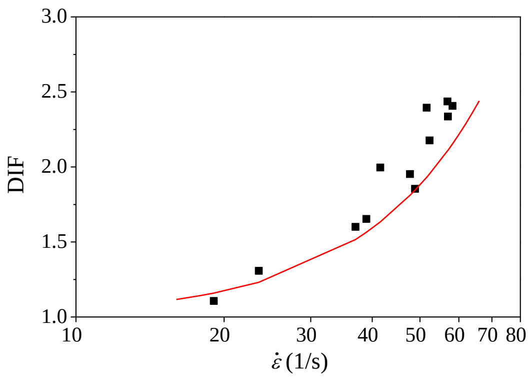

(b) RAC-30

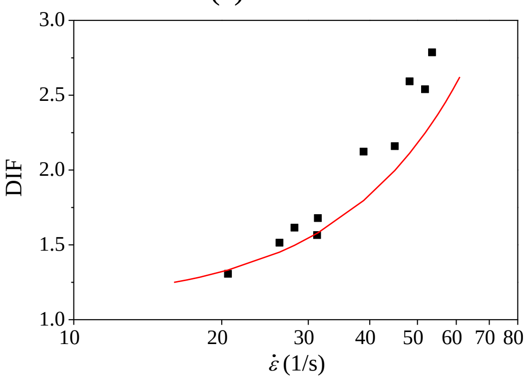

(c) RAC-70

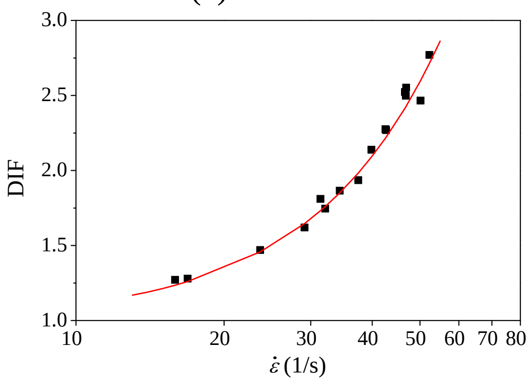

(d) RAC-100

Fig. 8 DIF - strain rate curve

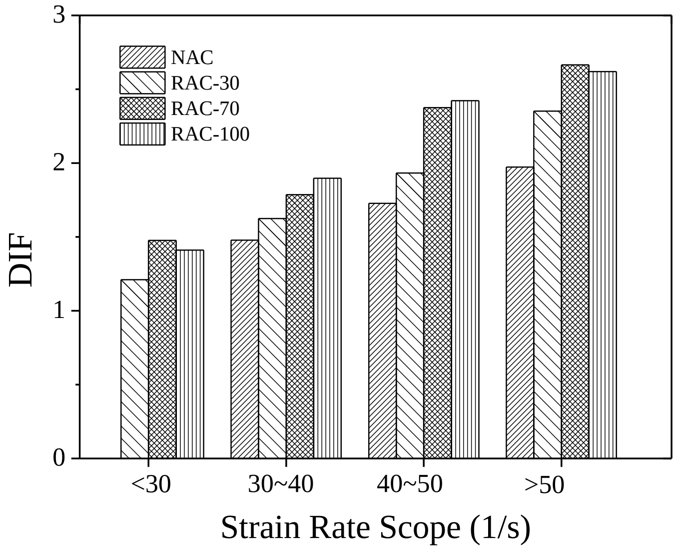

Fig. 9 DIF - strain rate scope

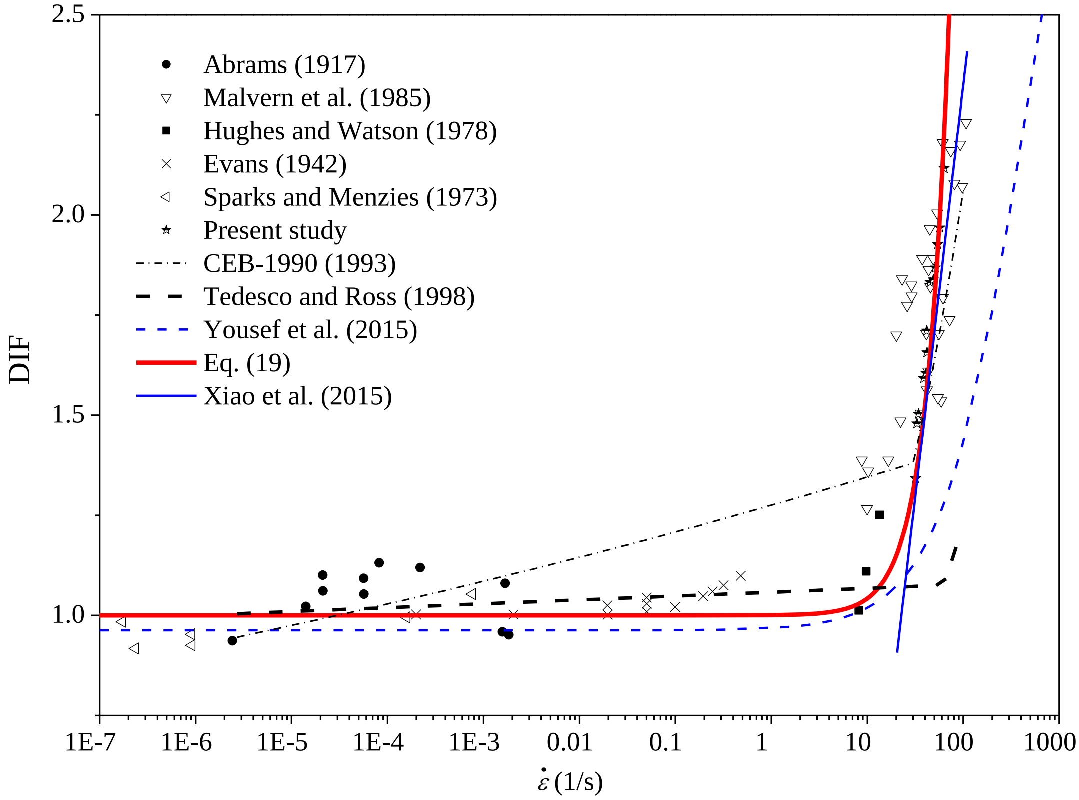

Fig. 10 DIF - strain rate curve for natural concrete

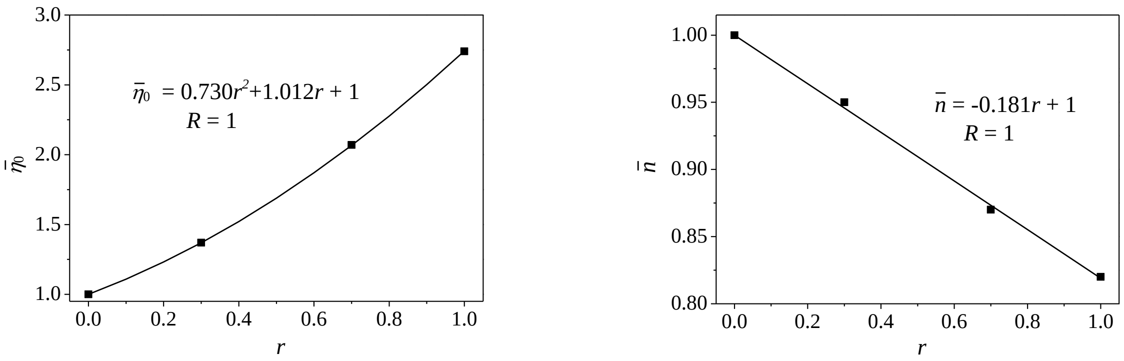

(a) $\bar{\eta}_0$ (b) $\bar{n}$

Fig. 11 Parameter $\bar{\eta}_0$ and $\bar{n}$ regression

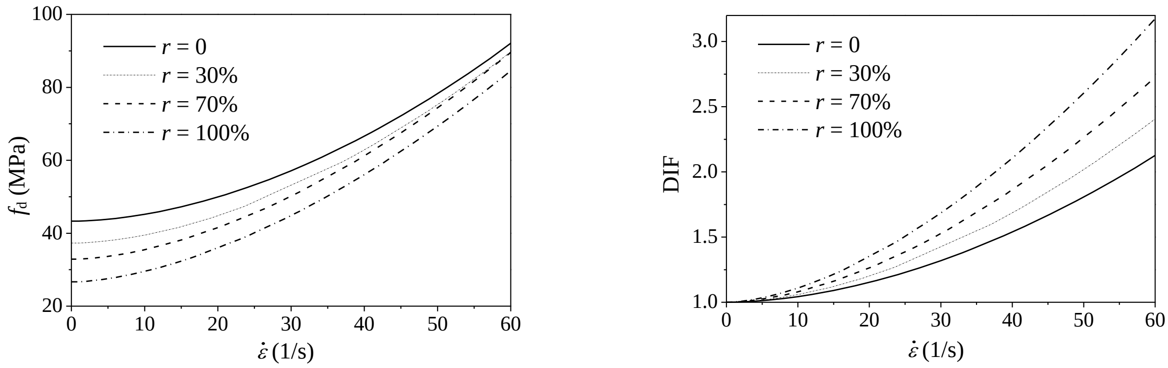

(a) Dynamic compressive strength - strain rate (b) DIF - strain rate

Fig. 12 Curves of regression formulae

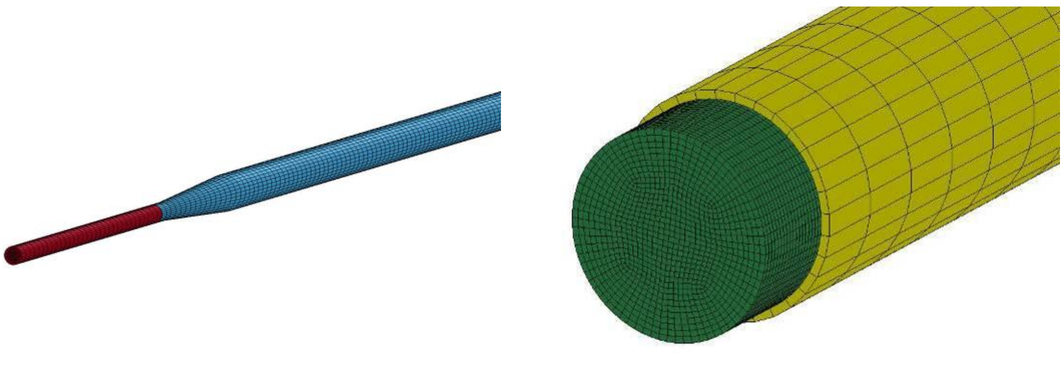

(a) Striker and incident bars (b) Specimen and transmitter bar

Fig. 13 FE model of SHPB test

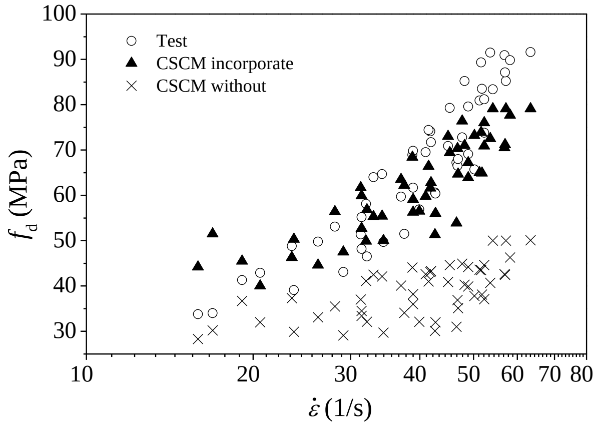

Fig. 14 Comparison between test and numerical simulation